JOURNAL OF SPACECRAFT AND ROCKETS
Vol. 35, No. 6, November–December 1998

Hypersonic Blunt-Body Flows in Hydrogen–Neon Mixtures

R. J. Stalker* and B. P. Edwards†
University of Queensland, Brisbane, Queensland 4072, Australia

The use of hydrogen–neon gas mixtures for experimental simulation of hypersonic ionizing blunt-body flows in hydrogen–helium atmospheres is considered. An existing approximate theory of blunt-body similarity is employed, and it is found that the ionizing relaxation of hydrogen can be accommodated in that theory if the effect of ionization along streamlines is correlated by a binary reaction variable involving the hydrogen partial pressure. The correlation is identical for helium and neon and is not influenced by the fraction of diluent. Thus blunt-body flows of hydrogen–helium mixtures can be simulated with hydrogen–neon mixtures of a different diluent fraction. The simulation is demonstrated by using experiments with a 60% hydrogen–40% neon mixture in a free piston nonreflected shock tunnel to obtain the shock shape on a hemispherically blunted cone entering the atmosphere of Uranus or Neptune.

Nomenclature

a = nose radius, m
I_D = diluent ionization energy, eV
I_H = hydrogen ionization energy, eV
k = Boltzmann's constant, eV/K
k_f = forward rate constant, m^3 $mole^{-1}$ s^{-1}
L = typical body dimensions, m
m = particle mass, kg
n = particle number density, m^{-3}
$(\dot{n}_e)$ = rate of electron density change, m^{-3}/s
p = pressure, Nm^{-2}
q = streamline velocity, m/s
r = molecular fraction of hydrogen
s = distance along streamline, m
T = temperature, K
U_∞ = freestream velocity, m/s
u, v, w = velocity components, m/s
v_e = root-mean-square random electron velocity, m/s
x, y, z = Cartesian coordinates
α = incidence of reference plane, deg
Δ = shock standoff, m
ε = inverse shock density ratio
θ_s = shock angle, deg
λ = bremsstrahlung energy loss, eV m^{-3} s^{-1}
ρ = density, kg/m^3
σ_{ej} = electron-heavy particle elastic energy transfer cross section, m^2
ϕ = density/normal shock density
χ = binary reaction variable, Nm^{-2} s
Ω = binary scaling parameter, Nm^{-2} s

Subscripts

D = diluent
e = electron
H = hydrogen
j = heavy particles
n = normal shock
s = shock

Presented as Paper 98-0799 at the AIAA 36th Aerospace Sciences Meeting and Exhibit, Reno, NV, Jan. 12–15, 1998; received Jan. 31, 1998; revision received July 10, 1998; accepted for publication July 15, 1998.

*Emeritus Professor, Department of Mechanical Engineering. Associate Fellow AIAA.

†Research Assistant, Department of Mechanical Engineering; currently Manager, Mill Engineering Technical Support, Sugar Mills Group, CSR, Ltd., Townsville, Queensland 4810, Australia.

Introduction

JUPITER and the other outer planets of the solar system are so different from the inner planets that they will afford rewarding exploration opportunities for many decades to come. Realizing these opportunities can be expected to sustain interest in missions involving the fluid mechanics of flight in hydrogen–helium atmospheres. The trend to smaller and cheaper vehicles for planetary exploration will call for the design of more efficient heat shields, and a demand for more sophisticated missions could lead to the use of lifting blunt bodies for aerobraking. Also, it is by no means certain that the 90-deg hemispherically blunted cone presently favored for high-energy atmospheric entry is the most efficient configuration that can be used. Developing an improved understanding of the fluid mechanics relevant to such configurations would make it easier to improve their efficiency, and this could be done through experimentation in ground facilities, if suitable ones were available.

Flight in the hydrogen–helium atmospheres of the outer planets involves velocities such that dissociation and ionization of hydrogen may have significant effects on the fluid mechanics of blunt-body flowfields. For example, nonequilibrium ionization is important because the high reaction rates at which it occurs ensure that the endothermic effects associated with ionization can produce significant changes in the pressure distribution on a blunt body. Unfortunately, effects such as these cannot be simulated in a hydrogen–helium ground facility. For example, an 89% H_2–11% He mixture requires a velocity of approximately 20 kms^{-1} to produce near complete dissociation, with no ionization, of the hydrogen, and such velocities cannot be produced in a hypersonic facility, having been achieved only with arc-driven shock tubes.[1]

An alternative to the use of hydrogen–helium mixtures is to replace the helium with neon. Neon has a molecular weight five times that of helium and, if it is used in sufficient concentrations, it increases the molecular weight of the test gas mixture to an extent that allows blunt-body flows with dissociating and ionizing hydrogen to be produced at velocities that can be achieved in hypersonic facilities. These velocities are indicated by Fig. 1, which shows the shock speeds measured in the shock tube of the free piston nonreflected shock tunnel T3 at the Australian National University, Canberra. With a 60% H_2–40% Ne mixture, complete dissociation is achieved with a freestream velocity of 9 kms^{-1}, which, with this shock tunnel, requires a shock speed of 8 kms^{-1}. This velocity is exceeded over a substantial range of initial densities, implying that sufficient stream energy is available to produce ionization as well as dissociation.

Neon also has the advantage that its atomic energy levels are well separated from those of hydrogen. The ionization potentials for hydrogen, neon, and helium, respectively, are 13.6, 21.6, and 24.6 eV. Ionization of these atoms takes place from the lowest excited state, the corresponding excitation potentials being 10.2, 16.6, and 21.0 eV, respectively. The excitation and the ionization potentials of neon and helium are sufficiently in excess of those of

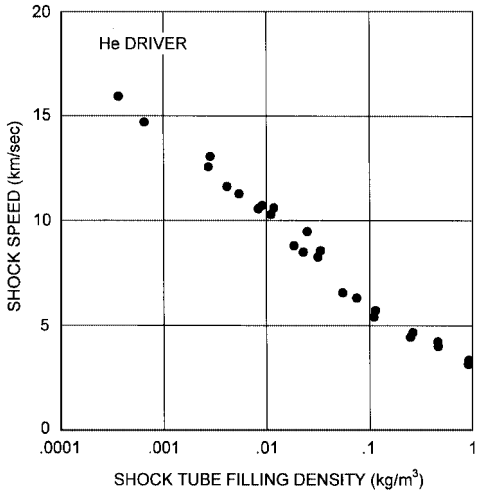

Fig. 1 Shock tube performance measured in free piston facility T3.

hydrogen to suggest that, up to relatively high temperatures, both will act as an inert diluent for the hydrogen ionization process. This may be contrasted with the expected behavior of argon, which has an ionization potential of 15.8 eV and an excitation potential of 11.6 eV. These potentials are sufficiently close to those of hydrogen to ensure that, in a hydrogen–argon mixture, hydrogen ionization would be accompanied by significant argon ionization.

This paper will investigate the simulation of hydrogen–helium inviscid blunt-body flows at hypersonic speeds by using hydrogen–neon mixtures. Nonequilibrium ionizing flows are emphasized because they are expected to generate more pronounced aerodynamic effects than dissociating flows. For ionizing flows, the dissociation of hydrogen is essentially complete close to the bow shock, and so it does not play an essential role in the blunt-body flows considered here. The paper begins by reviewing a previous approximate treatment of similarity in blunt-body flows and employs this as a framework for discussion of the use of hydrogen–neon mixtures to simulate hydrogen–helium blunt-body flows. Then experiments, in the nonreflected shock tunnel T3, on a 120-deg blunt cone using a 60% H_2–40% Ne mixture are reported, and it is shown how the results may be applied to a corresponding configuration in flight in a hydrogen–helium atmosphere by once again employing the blunt-body similarity theory.

Similarity of Blunt-Body Flows

Reference 2 reports a previous study of blunt-body flow similarity. This study considered scaling of blunt-body flows by investigating the manner in which freestream and model parameters could be varied to produce shock layer flows that were similar. The similarity meant that the distribution of variables (such as density, pressure, and velocity) in one shock layer flow could be obtained from that in another by appropriate choice of the freestream and model parameters. Blunt bodies of a generalized shape at incidence were considered, as shown in Fig. 2. A reference plane was located in the body, with Cartesian coordinates x, y, and z chosen such that y was normal to the reference plane. The incidence α was defined as the angle between the reference plane and the freestream flow direction. It was found that, neglecting terms of the order of ε_n^2, similarity between two such blunt-body flows could be obtained if the y coordinates were adjusted so that

$$\left\{\frac{1-\varepsilon_{n1}}{\varepsilon_{n1}}\right\}^{0.5} y_1 = \left\{\frac{1-\varepsilon_{n2}}{\varepsilon_{n2}}\right\}^{0.5} y_2 \qquad (1)$$

where the subscripts 1 and 2 refer to the two bodies. The similarity is subject to the following conditions:

1) As requirement 1, $\cos\alpha$ and the slope of the bow shock, in x, y, and z coordinates, were of order ε_n. Although this implies that the slope of the body surface and the angle of incidence must be small, it is not considered to be a serious limitation in the present application because these are conditions that will yield minimum heat transfer for given drag, as required for an efficient heat shield.

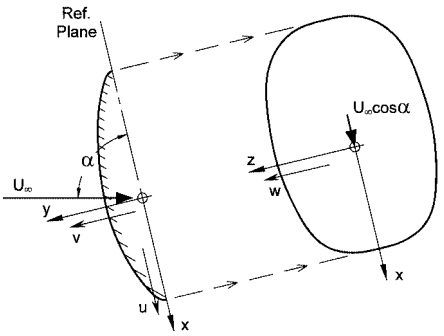

Fig. 2 Blunt-body configuration.

2) As requirement 2, $[(1-\varepsilon_n)/\varepsilon_n]^{0.5}\cos\alpha$ is the same in the two flows, i.e., the angle of incidence is also adjusted according to the normal shock density ratio.

3) As requirement 3, $\varepsilon_s/\varepsilon_n$ is the same for the same value of $\{[(1-\varepsilon_n)/\varepsilon_n]^{0.5}\times\theta_s\}$ in the two flows, where θ_s is the shock angle with respect to the reference plane. This condition is not difficult to satisfy for a perfect gas at high Mach numbers because ε_s is then insensitive to small changes of shock angle. However, for a chemically reacting gas, such as that considered here, ε_s may be expected to vary with changes in the shock angle, and this condition usually will be satisfied only approximately.

4) As requirement 4, the variation of ϕ along streamlines is the same for the two flows. For a perfect gas, or for a flow in chemical equilibrium, ϕ is effectively constant in the shock layer. For chemical nonequilibrium, the situation is more complicated and will be discussed further.

This similarity was found to provide a satisfactory correlation of shock shapes for perfect gas flows over a flat-faced cylinder, with ε_n ranging from 3.7^{-1} to 18.3^{-1}, and over spherically blunted cones with an included vertex angle exceeding 100 deg.

Hydrogen–Neon and Hydrogen–Helium

Satisfying requirement 4 for reacting nonequilibrium flows depends on the type of reaction. For reactions that proceed according to a rate given by binary kinetics, Gibson and Marrone[3] have shown that a shock-mapping technique may be applied to blunt-body flows, allowing an inviscid blunt-body flowfield to be built up from normal shock flows. Reference 2 discusses the scaling of dissociating blunt-body airflows in this context, and the discussion could be applied to flows with hydrogen as the dissociating constituent.

For nonequilibrium ionization of hydrogen in neon or helium diluents, however, binary kinetic behavior is not immediately apparent. The ionization of hydrogen involves two distinct steps. In the first step, the helium or neon diluent acts as a collision partner for electronic excitation. The second step occurs once sufficient electrons have been generated, and hydrogen–electron collisions come to dominate the ionization process. Therefore, it is not clear how the diluent concentration affects the overall rate process.

A further complication is the dependence of the electron–hydrogen atom ionization rate on the temperature of the electrons, a quantity that is different from the heavy particle temperature. Electron temperature is dependent on all components of the flow, and the variation of electron temperature is difficult to predict a priori.

Therefore, numerical methods were employed to investigate ionization relaxation along a streamline in the gas mixtures of interest. An existing computer program[4] was modified for the purpose. Equations for conservation of momentum, energy, and species were used, together with an equation defining the electron temperature,[5] i.e.,

$$1.5n_e q k\frac{\mathrm{d}T_e}{\mathrm{d}s} + n_e k T_e\frac{\mathrm{d}q}{\mathrm{d}s} = 3n_e m_e \bar{\nu} k(T - T_e)$$
$$- I_{\mathrm{H}}(\dot{n}_e)_{\mathrm{H}} - I_D(\dot{n}_e)_D - \lambda$$

where

$$\bar{\nu} = \sum_j \sigma_{ej} n_j \frac{v_e}{m_j}$$

The bremsstrahlung energy loss term λ was found to have a negligible effect on the results of the computation. Other radiative energy losses were negligible in comparison with λ.

The ionization reactions for hydrogen with their forward rate constants[6] were

$$H + M \rightarrow H^+ + M + e \qquad (M = H, Ne, He)$$

$$k_f = 6.2 \times 10^{16} T^{0.5} \exp(-10/kT) \text{ m}^3 \text{ mole}^{-1} \text{ s}^{-1}$$

$$H + e \rightarrow H^+ + 2e$$

$$k_f = 4.1 \times 10^{19} T_e^{0.5} \exp(-10/kT_e) \text{ m}^3 \text{ mole}^{-1} \text{ s}^{-1}$$

For neon and helium,[7]

$$Ne + e \rightarrow Ne^+ + 2e$$

$$k_f = 2.2 \times 10^{19} T_e^{0.5} \exp(16.9/kT_e) \text{ m}^3 \text{ mole}^{-1} \text{ s}^{-1}$$

with the identical reaction for helium, except that the activation energy becomes 20 eV. Hydrogen–electron elastic cross sections were calculated from[7]

$$\sigma_{H,e} = 3.95 \times 10^{-19} \exp(-0.589 kT_e) \text{ m}^2$$

The helium–electron elastic cross section was taken as 6.5×10^{-20} m^2 (Ref. 8), and the neon–electron cross section was fitted to data in Ref. 8 by

$$\sigma_{Ne,e} = 1.0 \times 10^{-20} (0.41 \log T - 2.24) \text{ m}^2$$

The resulting computer program was run for a series of cases in which the pressure remained constant along the streamline downstream of the shock. At flow energies such that significant ionization takes place, the dissociation of hydrogen is completed close to the shock, and therefore the computations were started at the shock with the hydrogen completely dissociated. Results are presented using the binary reaction variable

$$\chi = \int \frac{rp}{q} \, ds \tag{2}$$

where r is the molecular fraction of hydrogen in the gas mixture in the absence of dissociation and ionization.

Results are shown in Figs. 3 and 4 for a range of postshock temperatures, corresponding to differing streamline enthalpies. It was found that there was no detectable difference in the use of neon or helium as diluent, except when approaching equilibrium at the highest temperature in Fig. 4, where the ionization of neon took place. Figure 3 shows that the binary reaction variable based on the hydrogen partial pressure provides a good correlation during the relaxation process and shows the weak effect that the amount of diluent has on the relaxation process until it approaches equilibrium. Figure 4

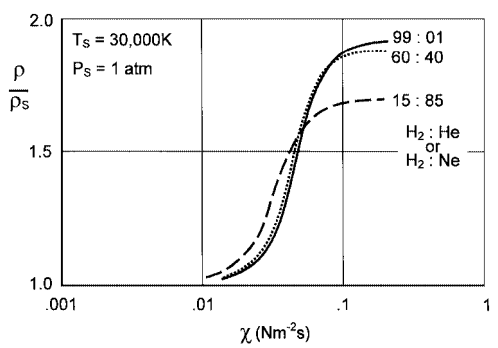

Fig. 3 Ionizing relaxation: effect of diluent concentration.

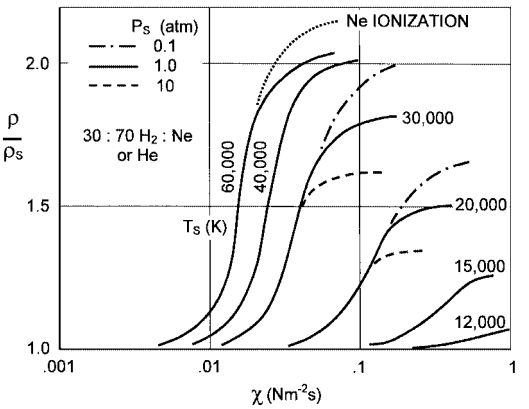

Fig. 4 Ionizing relaxation: effect of temperature and pressure.

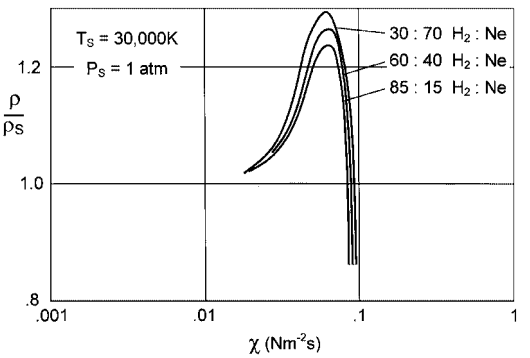

Fig. 5 Ionizing relaxation in a negative streamwise pressure gradient.

shows the effect of temperature and pressure at one mixture ratio. Again the binary reaction variable is effective in correlating the rise in density during the relaxation process, but because the equilibrium density varies with pressure, curves at different pressure levels diverge as they approach equilibrium. As would be expected, the overall relaxation distance reduces with increasing temperature.

For a streamline that passes over a body to a region of lower pressure, a reduction in the streamline enthalpy will occur. Figure 5 shows the effect of a pressure gradient, which causes the streamline enthalpy to be reduced by 15% in passing from the shock wave to the point at which the density has been reduced to the value at the shock. This enthalpy reduction roughly corresponds to a halving of the pressure. Once again, the binary reaction variable correlates the curves; in this case, though, there is a small effect of mixture ratio.

Thus, the nonequilibrium variation of the density ratio ρ/ρ_s with the hydrogen binary reaction variable is, for a given postshock temperature, independent of whether neon or helium is used as a diluent and, to a good approximation, is independent of the amount of diluent used. It can be readily shown that, if a blunt-body flow is such that requirement 1 of the preceding section is satisfied, the postshock streamline enthalpy is uniform across the body to within $\mathcal{O}(\varepsilon_n)$ and, therefore, the postshock temperature may be taken as uniform. Then, provided that requirement 3 is satisfied, the analysis of Ref. 2 shows that requirement 4 is also satisfied if the modified binary scaling parameter

$$\Omega = \frac{rp_n L[\varepsilon_n(1-\varepsilon_n)]^{-0.5}}{U_\infty} \tag{3}$$

is the same in the two flows. Then, with an appropriate choice of freestream and model parameters, a hydrogen–neon blunt body flow can be generated that is similar to a hydrogen–helium flow with a different mixture ratio.

For postshock temperatures exceeding 20,000 K, the dissociation of hydrogen may not be effectively complete when ionization begins. This may affect the electron temperature, and the rate of ionization of hydrogen, through the excitation of molecular energy modes of hydrogen by electrons and, therefore, may somewhat modify the curves in Figs. 3–5. However, the electron collision processes

involved are binary in nature and, when combined with the binary scaling behavior apparent in Figs. 3–5, may be expected to yield modified curves that show the same binary scaling behavior as the original curves.

Experiment

Shock Tunnel and Test Conditions

Experiments were conducted in the free piston shock tunnel T3 at the Australian National University. The shock tunnel involved a compression tube 6 m long and 300 mm in diameter driving a shock tube 8 m long and 76 mm in diameter. The piston mass was 90 kg. The tunnel was operated in the nonreflected mode with a prior steady flow. The features of the prior steady flow technique, as they were realized in the shock tunnel, are detailed in Ref. 9 and will be only briefly described here.

Figure 6 shows a schematic arrangement of the shock tunnel configured for prior steady flow nonreflected operation, as well as the hypersonic nozzle and test section in more detail. The prior steady flow of test gas through the nozzle is initiated by opening a valve (not shown) downstream of the test section through recoil of the shock tunnel assembly brought about by the piston undergoing its compression stroke. This allows the prior steady flow in the nozzle to become established before the primary shock wave arrives. The nozzle feed tank, which surrounds the nozzle and the downstream 1.8 m of the shock tube, is initially filled with test gas at the same pressure as in the shock tube and thus serves to maintain the shock tube pressure, as test gas is supplied to the nozzle, in the time interval before the test flow begins.

Use of the prior steady flow technique eliminates the necessity for a diaphragm at the entrance to the hypersonic nozzle, while allowing the disturbances associated with the flow starting process to be swept through the nozzle as rapidly as is theoretically possible with a diaphragm.[9] Its use confers two advantages. One is that diaphragm fragments in the nozzle may delay completion of the nozzle flow starting process, and the other is that the purity of the test gas is maintained at the initial filling level.

The contoured axisymmetric hypersonic nozzle had an inlet diameter of 38 mm and, though it was designed to produce uniform flow at an area ratio of 16, it was truncated at an exit diameter of 130 mm to facilitate flow starting. The nozzle contour was designed to produce satisfactory flow over a range of shock tube filling pressures with a 60%:40% hydrogen–neon mixture.[10] When the nozzle was calibrated by bar gauge pitot surveys, it was found to produce a flow with no more than 2-deg divergence over the test region.[10]

The experiments were performed with a 60%:40% hydrogen–neon mixture. This mixture ratio was chosen because, as shown in Fig. 3, the density variation with χ closely follows, through the relaxation region into equilibrium, that of a 99%:1% hydrogen–helium mixture and, therefore, will follow that for mixtures with 10–15% of helium, which is typical of the atmospheres of the outer planets. With a 60%:40% hydrogen–neon mixture, it is possible to produce equilibrium blunt-body flows in the shock tunnel and, though this paper concerns nonequilibrium flows, it was considered worthwhile gaining tunnel experience with this mixture ratio.

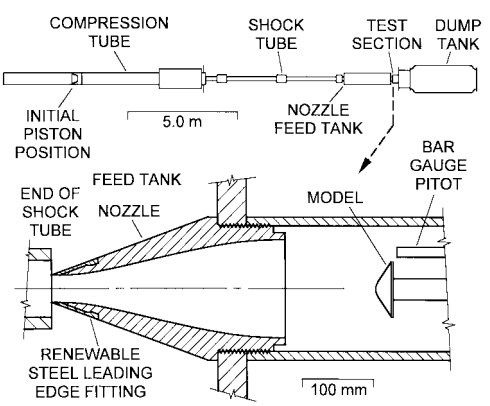

Fig. 6 Free piston shock tunnel with prior steady flow nonreflected modification.

Table 1 Shock tube test conditions: test gas 60:40 H_2/Ne

Test condition	Error, %	1	2	3	4
Shock tube filling pressure, kPa	±1	5.32	2.66	1.33	0.664
Shock speed, km · s^{-1}	±3	8.3	9.3	10.0	11.1
Stagnation enthalpy, MJ · kg^{-1}	±6	63	79	91	109

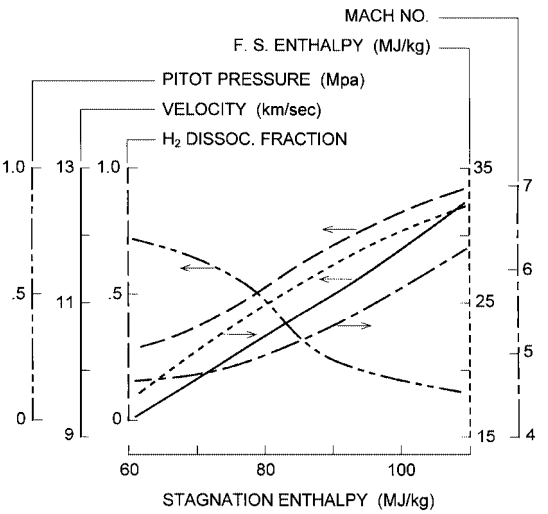

Fig. 7 Test flow: 60% H_2:40% Ne.

The experimental conditions are set out in Table 1 and were chosen such that test section densities were high enough to allow schlieren photography of model flows. Helium driver gas was used throughout the experiments, with a diaphragm rupture pressure of 75 MPa and a driver gas volumetric compression ratio of 83, to yield a nominal driver gas temperature of 5560 K.

The test section conditions were obtained by using the shock speed and the filling pressure to calculate the postprimary shock equilibrium conditions and by subsequently employing a computer program for a one-dimensional nonequilibrium nozzle expansion from these conditions to a nozzle area ratio of 16. The postprimary shock degree of ionization never exceeded 1% and, as it was not expected to have a large effect on the test flow, electron recombination was modeled by a one-temperature rate equation. The resulting test section flow properties are shown in Fig. 7. The Mach number presented in Fig. 7 was based on the nonequilibrium speed of sound in the test section.

Instrumentation and Flow Calibration

The model was a spherically blunted cone, of 120-deg vertex angle, with a base diameter of 80 mm and a nose radius of 20 mm. The shock formed about the model was photographed with a double-pass schlieren system, using a dye laser light source, of 5-ns pulse duration, which yielded a peak output at 590 nm. In spite of the use of a filter of 3.6-nm bandwidth, difficulty was experienced in eliminating background flow luminosity from the image, and it was necessary to accept a degree of masking of the knife edge, which somewhat downgraded the image definition.

Test times were determined by using a John Hadland Imacon-790 image converter camera, operating in the streak mode, to take time-resolved spectra of the radiation from the stagnation region of a 50-mm-diam hemisphere mounted in the test section. The results are shown in Fig. 8a, with the time t measured from the time of flow arrival, which is taken as the time of arrival of the primary starting shock at the stagnation point of the model. The two hydrogen spectral lines, H_α and H_β, are clearly visible at test condition 4 and 12 μs later are joined by an array of spectral lines that are thought to arise from driver gas impurities in the contact region. The appearance of impurities was taken as the end of the test time, although streak photographs of the luminous shock layer in the stagnation region indicate that the shock standoff remains constant for much longer times. For the other test conditions, the spectral lines of hydrogen become progressively less intense as the stagnation enthalpy

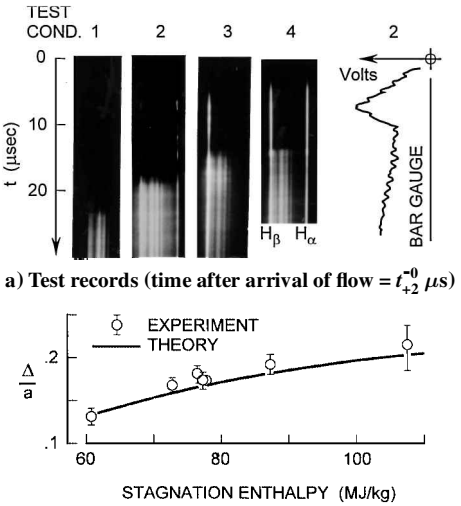

a) Test records (time after arrival of flow = t_{+2}^{-0} μs)

b) Shock standoff

Fig. 8 Test flow calibration.

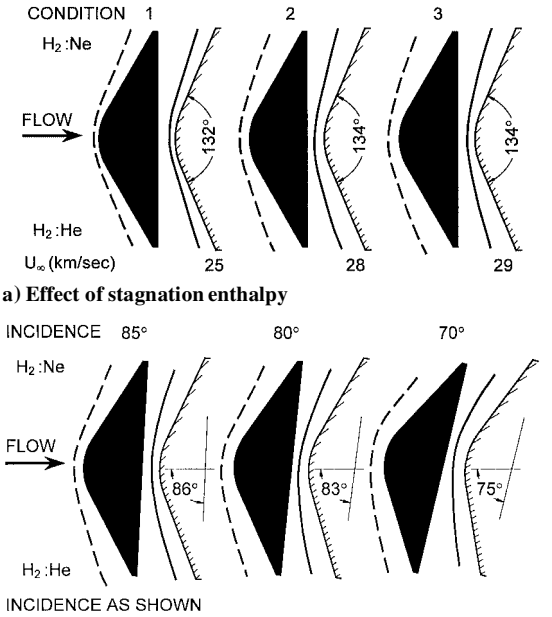

a) Effect of stagnation enthalpy

b) Effect of incidence, test condition 2

Fig. 9 Experimental simulation of flight in 85% H_2:15% He atmosphere with 60% H_2:40% Ne test gas mixture.

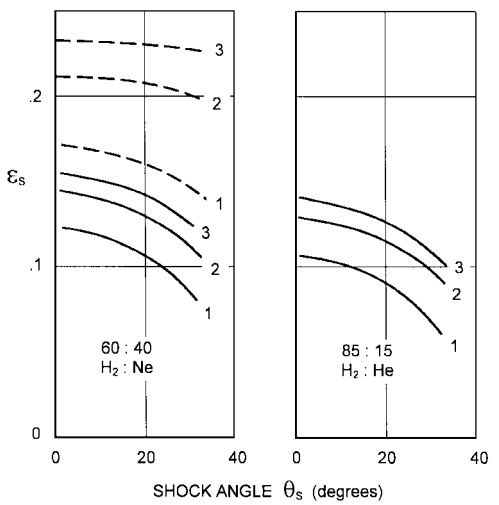

Fig. 10 Inverse shock density ratio; effect of shock angle, postnormal shock temperatures matched at conditions 1, 2, and 3: – – –, experimental conditions, and ——, upstream enthalpy = 0.

is reduced, but the impurity radiation remains to indicate the end of the test time. All of the schlieren images discussed subsequently were obtained during the test time.

Also shown in Fig. 8a is a pitot record, obtained using a bar gauge 12.7 mm in diameter, with a 2-μs rise time, located at a radial distance of 12 mm outside the edge of the model and 8 mm downstream, as shown in Fig. 6. The bar gauge was, therefore, within the downstream flow from the shock layer on the model. It can be seen that the pitot pressure reaches a near constant value 10 μs after flow arrival, thus providing a qualitative indication of steady flow in the shock layer. This was confirmed by a series of schlieren photographs of the cone flow at test condition 2, which showed a shock that remained steady (to within ±4% of the distance from the model surface) from 13 μs until at least 18 μs after flow arrival. This 5-μs interval represented the time for the flow to pass halfway along the flank of the model, indicating that there was adequate time for significant flow unsteadiness to be evident. At test conditions 1 and 3, the schlieren photographs were taken at times close to the end of the test times indicated in Fig. 8a. By taking the period of unsteady model flow to be inversely proportional to the test flow velocity, it could be ascertained that the schlieren photographs at these conditions were also taken when the shock was steady.

The normal shock density ratio was checked from the schlieren images by measuring the shock standoff at the nose of the models. Estimates indicated that the postshock sonic point occurred on the spherical portion of the models, and therefore the shock standoff could be taken as that on a sphere. Further, because dissociation was completed within 0.2 mm of the shock, and ionization caused a rise in density of less than 10% within 5 mm of the shock, it was a good approximation to assume constant density in the shock layer near the nose. The shock standoff could then be predicted by the use of existing correlations between shock standoff and density ratio for a sphere[11] and is presented in Fig. 8b. The satisfactory agreement between the experimental measurements and predictions confirms that the test flow produces the expected normal shock density ratios.

Results and Discussion

Although the schlieren images of the shock could be clearly identified in the photographs, it was doubtful that these could be suitably reproduced in published form. Therefore, the image of the shock was outlined with a fine black pen before the photograph was traced, recorded digitally, and printed out with a computer, to produce a black-and-white copy of the photograph. Copies of the schlieren photographs obtained in this manner are presented in Fig. 9 with the model profile shown in black.

Figure 9a shows the bow shock with the model at zero incidence for test conditions 1–3. It can be seen from Fig. 7 that there is significant freestream enthalpy, arising from both the freestream temperature and the dissociation of hydrogen in the freestream. The effect this has on ε_n, the inverse normal shock density ratio, is shown, for $\theta_s = 0$ deg, in Fig. 10, where the values of ε_s under tunnel conditions are compared with those that would be obtained with zero freestream enthalpy, corresponding more closely to the flight condition. The comparison has been made for the same values of postshock temperature with complete hydrogen dissociation, i.e., for temperatures of 8920, 12,120, and 15,640 K for test conditions 1, 2, and 3, respectively. Figure 10 also includes values of ε_s for a 85% H_2:15% He mixture at zero freestream enthalpy and the same postshock temperatures. It is seen that they are little different from those obtained with the 60% H_2:40% Ne mixtures under the same conditions, showing that the difference in ε_s values between the hydrogen–neon mixture of the experiments and the hydrogen–helium mixture is due principally to the freestream enthalpy in the tunnel.

Using the transformation of Eq. (1) and the values of ε_n of Fig. 10, Fig. 9a could be used to obtain the shock shape for blunt cones producing a similar shock layer flow in the hydrogen–helium mixture. These are also presented in Fig. 9a, each one adjacent to the copy of the photograph from which it was derived. The model surface is shown crosshatched for the hydrogen–helium flows.

The validity of the similarity in these cases may be checked by noting the requirements listed in the second section, particularly requirements 3 and 4. Calculations show that the variation of $\varepsilon_s/\varepsilon_n$ with $(1-\varepsilon_s/\varepsilon_n)^{0.5}\theta_s$, i.e., with distance from the centerline, is identical to within 6% for each pair of flows, thereby closely satisfying requirement 3. The calculations also show that postshock temperatures are the same, to within 1.5%, and therefore the variation of ϕ along streamlines is the same if the binary scaling parameter, given by Eq. (3), is also the same. Adjustment of the binary scaling parameter can be readily achieved by adjusting the freestream pressure. Thus, requirement 4 is also satisfied, and it can be concluded that to within $\mathcal{O}(\varepsilon_n)$ each hydrogen–helium flow is indeed similar to its corresponding hydrogen–neon flow.

Effects of hydrogen dissociation are evident in the shock shapes for hydrogen–neon (and the associated hydrogen–helium flows), particularly as they relate to shock detachment. Shock detachment occurs when the shock layer on the cone flank becomes subsonic and is marked by general movement of the shock away from the body. The normal shock density ratios are such that, in a perfect gas, shock detachment should occur at cone semiangles of 57, 54, and 52 deg for test conditions 1, 2, and 3, respectively, and as these values are substantially smaller than the model flank semiangle of 60 deg, it follows that perfect gas behavior would lead to the enlarged standoff distances typical of a detached shock. However, the measurements in Fig. 8b of shock standoff distance at the nose indicate that shock detachment is not occurring at test condition 1, and this is reinforced by the shock profile being straight along the flanks. Also, when the shock profile at this condition was compared with that obtained by interpolating between calculations for detached perfect gas flow over the same body shape, to yield the profile at the same normal shock density ratio,[12,13] it was found that the separation between the shock and the body was only 60–70% of that of the perfect gas case. Because temperatures at test condition 1 are too low for significant ionization, it is concluded that dissociation of hydrogen close to the shock lowers the temperatures in the shock layer to a level such that the flow on the conical flank of the model is supersonic, and a detached flow does not develop.

The measurements in Fig. 8b are also consistent with attached shock flow for test conditions 2 and 3, though the shock is curved on the conical flanks. In a perfect gas, this would be consistent with a flow approaching detachment.[12] However, at these conditions, the shock layer temperatures are sufficient to cause significant ionization and, if the data plotted in Fig. 7 are used, together with the Newtonian approximations, the values of χ reached on a streamline traversing the conical flank are 1.2 and 0.6 Nm^{-2} s for test conditions 2 and 3, respectively. Reference to Fig. 4 and the postshock temperatures just noted indicate that ionization will cause density changes of up to 20% on such a streamline, and the associated reduction in stream-tube area will result in shock curvature such as that observed. Thus, it is possible that ionization may contribute to the shock curvature.

The effect of incidence is demonstrated in Fig. 9b, where copies of schlieren photographs are presented of the same model at varying angles of incidence at test condition 2. The similar hydrogen–helium flow, shown with each copy, is for an angle of incidence that satisfies requirement 2. Because the angle the shock makes with the freestream reaches higher values toward the trailing edge of the model surface than in Fig. 9a, requirement 3 is not satisfied as closely, the variation of $\varepsilon_s/\varepsilon_n$ with distance from the model centerline differing by as much as 23% for corresponding flows. On the other hand, the postshock temperatures agree within 5%, indicating that requirement 4 is more closely satisfied. Thus, the simulation achieved with the hydrogen–neon mixture at 20-deg incidence will be less accurate that at zero incidence.

The schlieren copy of Fig. 9b, at 85-deg incidence, exhibits the same shock shape with respect to the body as that of Fig. 9a, at 90-deg incidence. This similarity of shock shapes accords with the usual experience with shock attached flow on cones, where the shock tends to rotate with the cone as it is varied through small angles of incidence. Further rotation to incidence angles of 80 and 70 deg sees shock standoff distance increase at the nose without significant change near the outer edge of the forward flank. This invariance of the forward flank shock standoff may be, at least partly, because of more extensive ionization arising from the higher temperatures following the near normal shock in that region, but it may also be because the flow is becoming increasingly three dimensional at these angles of incidence.

The freestream velocities are noted for each of the hydrogen–helium flows of Fig. 9a and encompass the maximum entry velocities used in a recent study of entry into the atmospheres of Uranus and Neptune.[14] By using the binary scaling parameter of Eq. (3), these hydrogen–helium model flows could be scaled to the flight situation. Shock shapes thus obtained for flight conditions can be significant because they provide an indication of the approach of shock detachment,[12] which can affect the aerodynamic stability of blunt bodies.

For the designer of atmosphere entry configurations, experiments such as these are likely to be useful for validation of computational fluid dynamics codes. As the simulation is approximate, care should be exercised when highly accurate knowledge of hydrogen–helium flows is required. For example, such a case could arise in locating the sonic line for a flow close to shock detachment. However, even in this case, validation of a code for hydrogen–neon flow will increase confidence in its use for hydrogen–helium flow.

The need to work at test section densities that allowed schlieren photography meant that shock tube filling densities greater than 2.7×10^{-3} kg/m^3 were required. As can be seen from Fig. 1, this limited the shock speed to approximately 11 km/s. It is evident from Fig. 1 that higher velocities can be produced, and therefore higher velocities in hydrogen–helium flows can be simulated, with attendant higher levels of hydrogen ionization, provided that techniques of flow visualization are available that are adequate for the lower densities involved.

It is also worth emphasizing that, although shock shapes can play an important role in the validation of computer codes,[15] the similarity between flows applies to the entire blunt-body shock layer. Therefore, other experimental data for hydrogen–neon flows, such as measurements of surface pressure or flow visualization based on optical emission, can be used for more complete validation of codes for hydrogen–helium flows.

Expansion tubes are being developed that yield flows at stagnation enthalpies as high, or higher, than is achieved in the nonreflected shock tunnel,[16] and these stagnation enthalpies are obtained with lower freestream enthalpies and longer test times. Thus, it is possible that expansion tubes may ultimately provide more accurate simulation than the nonreflected shock tunnel.

Conclusion

The study showed that hydrogen–neon mixtures could be used to simulate ionizing inviscid blunt-body flows in hydrogen–helium mixtures typical of the atmospheres of the large planets of the solar system. The simulation was approximate in that it made use of a previously published investigation of approximate blunt-body similarity and was most accurate when the angle between the normal to the body surface and the freestream direction was small. It involved adjustment of the shape of the body surface as the normal shock density ratio varied between the two flows. Similarity between the flows also required that density changes due to ionizing relaxation along streamlines follow a binary kinetics law, and this was found to be so if the partial pressure of hydrogen was used in the binary reaction variable. This applied whether the diluent was helium or neon and for a wide range of diluent fractions, thus making it possible to simulate blunt-body flows of hydrogen–helium mixture with hydrogen–neon mixtures of a different diluent fraction.

Experiments with a 60% H_2:40% Ne mixture in a nonreflected free piston shock tunnel demonstrated the use of the described simulation to obtain shock shapes about a hemispherically blunt cone. These shock shapes exhibited effects of hydrogen dissociation, but the effects of hydrogen ionization, if present, were masked by other features of the flow. The shock shapes were used to obtain shock shapes about such a blunt body at velocities encompassing those for entry into the atmospheres of Uranus or Neptune. The experiments were limited to these velocities by the need to work at test section

densities that allowed schlieren photography, but higher velocities can be simulated if this requirement is relaxed.

Acknowledgments

A grant from the Australian Research Council to conduct the experiments is appreciated. The authors are also grateful for the use of the T3 shock tunnel at the Australian National University and for the generous assistance with the experiments provided by the staff of the Physics Department there.

References

[1]Menard, W. A., "A Higher Performance Electric-Arc-Driven Shock Tube," *AIAA Journal*, Vol. 9, No. 10, 1971, pp. 2096–2098.

[2]Stalker, R. J., "A Similarity Transformation for Blunt Body Flows," AIAA Paper 86-0125, Jan. 1986.

[3]Gibson, W. E., and Marrone, P. V., "Correspondence Between Normal-Shock and Blunt-Body Flows," *Physics of Fluids*, Vol. 5, Dec. 1962, pp. 1649–1656.

[4]Lordi, J. A., Mates, R. E., and Moselle, J. R., "Computer Program for Numerical Solution of Non Equilibrium Expansion of Reacting Gas Mixtures," NASA CR-472, May 1966.

[5]Glass, I. I., and Liu, W. S., "Effects of Hydrogen Impurities on Shock Structure and Stability of Ionizing Monatomic Gases. Part 1 Argon," *Journal of Fluid Mechanics*, Vol. 89, Pt. 1, 1978, pp. 55–77.

[6]Stalker, R. J., "Shock Tunnel Measurement of Ionization Rates in Hydrogen," *AIAA Journal*, Vol. 18, No. 4, 1980, pp. 478–480.

[7]Liebowitz, L. P., "Measurements of the Structure of an Ionizing Shock Wave in a Hydrogen–Helium Mixture," *Physics of Fluids*, Vol. 16, No. 1, 1973, pp. 59–68.

[8]Massey, H. W. S., and Burhop, E. H. S., *Electronic and Ionic Impact Phenomena*, 2nd ed., Vol. 1, Oxford Univ. Press, London, 1969, p. 26.

[9]Stalker, R. J., and Mudford, N. R., "Unsteady Shock Propagation in a Steady Flow Nozzle Expansion," *Journal of Fluid Mechanics*, Vol. 241, Aug. 1992, pp. 525–548.

[10]Mudford, N. R., Stalker, R. J., and Shields, I., "Hypersonic Nozzles for High Enthalpy Non Equilibrium Flow," *Aeronautical Quarterly*, Vol. 31, May 1980, pp. 113–131.

[11]Hornung, H. G., "Non-Equilibrium Dissociating Nitrogen Flow over Spheres and Circular Cylinders," *Journal of Fluid Mechanics*, Vol. 53, May 1972, pp. 149–176.

[12]Calloway, R. L., and White, N. H., "Measured and Predicted Shock Shapes and Aerodynamic Coefficients for Blunted Cones at Incidence in Air at Mach 5.9," NASA TP-1652, May 1980.

[13]Miller, C. G., III, "Shock Shapes on Blunt Bodies in Hypersonic-Hypervelocity Helium, Air and CO_2 Flows, and Calibration Results in Langley 6-inch Expansion Tube," NASA TN-D-7800, Feb. 1975.

[14]Tauber, M., Wercinski, P., Henline, W., Patterson, J., and Yang, L., "Uranus and Neptune Atmospheric-Entry Probe Study," *Journal of Spacecraft and Rockets*, Vol. 31, No. 5, 1994, pp. 799–805.

[15]Boyce, R. R., Morton, J. W., Houwing, A. F. R., Mundt, C., and Bone, G. J., "Computation Fluid Dynamics Validation Using Multiple Interferometric Views of a Hypersonic Flowfield," *Journal of Spacecraft and Rockets*, Vol. 33, No. 3, 1996, pp. 319–325.

[16]Morgan, R. G., "A Review of the Use of Expansion Tube for Creating Superorbital Flows," AIAA Paper 97-0279, Jan. 1997.

J. R. Maus
Associate Editor